Lab on a Chip

Cite this: *Lab Chip*, 2012, **12**, 821

www.rsc.org/loc

PAPER

Ultrahigh sensitivity assays for human cardiac troponin I using TiO_2 nanotube arrays†

Piyush Kar,[b] Archana Pandey,[ab] John J. Greer[a] and Karthik Shankar*[b]

Received 15th September 2011, Accepted 8th December 2011
DOI: 10.1039/c2lc20892j

Rapid, highly sensitive troponin assays for the analysis of serum at the point-of-care are particularly desirable for the effective treatment of myocardial infarction (MYI). TiO_2 nanotube arrays constitute a low cost, high surface area, semiconducting architecture with great promise for biosensing applications due to their compatibility with multiple detection techniques. Using TiO_2 nanotube arrays functionalized with highly robust and ordered carboxyalkylphosphonic acid self-assembled monolayers, we have developed a simple and highly sensitive fluorescence immunoassay which can detect concentrations of human cardiac troponin I as low as 0.1 pg ml^{-1} without the use of enzymatic amplification. Varying the morphological parameters of the nanotube arrays allows tuning the detection range over 6 orders of magnitude of the troponin concentration from 0.1 pg ml^{-1}–100 ng ml^{-1}.

1. Introduction

The accurate quantification of the structural heart proteins cardiac troponin I and T has become integral to the diagnosis of acute myocardial infarction (AMI) due to AMI's direct role in the death of heart muscle tissue. Rapid identification of AMI or the absence thereof, in patients presenting with acute chest pain, is a key enabler of effective evidence-based medical treatment and management.[1] In this regard, a major deficiency of traditional assays for cardiac troponins (cTns) is inadequate sensitivity in the first few hours of AMI due to the significant delay occurring between the onset of ischemia and the increase in serum concentration of cTns.[1,2]

The promise of point-of-care (POC) biodiagnostic tests is to deliver the benefits of simple, fast and consistent testing and to allow prompt and effective decisions to be made on the course of treatment. The use of semiconductor nanowires and nanotubes in POC biomarker assays is motivated by their rapid response time, the large number and density of sensor elements and the high sensitivity achievable by exploitation of their morphological, optical and electronic properties.[3,4] Field-effect transistor sensors based on silicon nanowires and carbon nanotubes have been used to perform the label-free detection of cancer markers and DNA at picomolar concentrations.[5,6] In the case of highly ordered TiO_2 nanotube arrays (TNAs), the availability of electron percolation pathways, a high surface area, a large capacitance in solution,[7] tunable pore diameters[8] and well-defined controllable reflectance spectra ensure the compatibility of this assay platform with multiple detection techniques including but not limited to interferometric biosensing,[7] electrochemical impedance and amperometric sensing, immunoassays,[9] FRET-based biosensing and photoconductive and photoelectrochemical biosensing.[10] TNAs are also being researched for use in bone implants,[11,12] in drug-eluting stents,[13] in stem cell differentiation,[14,15] as biofiltration membranes[16] and as clotting enhancers in gauze pads for the control of hemorrhage.[17] TNAs constitute an air-stable and potentially self-cleaning and re-usable assay platform.[9] Perhaps more importantly, TNAs are fabricated at room-temperature by an inexpensive and scalable anodization process. A subsequent high temperature annealing step induces crystallinity and improves electronic properties but is not necessary for several types of assays based on this platform.

Assays based on nanostructures, for example, are now beginning to make the transition from the laboratory scale devices to clinical trials.[18] The diagnosis of the disease on the basis of concentration of certain biomolecules requires assays that can detect molecules of interest (in our case it is Troponin I) sensitively. In most of the cases the targets are either proteins or nucleic acids. There are basically two approaches by which high sensitivity can be achieved: 1) target-based amplification where the catalytic process is triggered by the recognition event and generates surrogates for that target with polymerase chain reaction being the best example,[19] and the second approach is 2) signal based amplification where a catalytic entity is used to amplify the signal that results from the binding site.[20] A typical example of signal based amplification is enzyme-linked immunosorbent assay (ELISA), where a target protein can be captured by the antibody and then sandwiched with a second antibody which is associated with a catalytic, signal generating entity.[21] Although there are advances in protein disease marker detection,

[a]*Department of Physiology, University of Alberta, Edmonton, AB, Canada*
[b]*Department of Electrical and Computer Engineering, University of Alberta, Edmonton, AB, Canada. E-mail: kshankar@ualberta.ca*
† Electronic supplementary information (ESI) available. See DOI: 10.1039/c2lc20892j

the current ELISA based detection methods have several drawbacks. First, a tiny ratio of protein to antibodies might reduce the sensitivity of the device. Secondly, the antibodies are floating on different surfaces randomly which may make proteins inaccessible to antibodies. Thirdly, because of their two-dimensional structures, all the antibodies might not capture the proteins thus contributing to lower sensitivity. A significant increase in detection sensitivity and signal to noise (S/N) ratio could be achieved if the following crucial improvements are made: (i) Increase in the density and the ratio of antibodies to protein, (ii) Efficient control of antibody orientation upon the surface immobilization of antibodies and (iii) A higher surface-to-volume ratio by using three-dimensional surfaces so that the antibodies can capture more proteins which leads to recurrent antibody-protein binding. In this regard, TiO_2 nanotube arrays constitute a highly promising architecture to overcome the drawbacks of ELISA-based methods and increase detection sensitivity.

Direct physisorption and chemisorption of proteins through the interaction of their charges and/or amine groups with the TiO_2 surface has been employed to immobilize biomolecules on TNAs.[9] However, the amine-TiO_2 linkage is relatively weak and electrostatic adsorption is a function of the TiO_2 surface preparation. In pursuit of a more robust binding of proteins and other biomolecules to the substrate while simultaneously exploiting the many desirable properties of the TNA architecture, several reports have used TNAs decorated with gold nanoparticles as assay platforms which provide access to thiolate SAM-based immobilization protocols.[10,22,23] Furthermore, assays based on planar gold films and gold nanoparticles and nanorods[24] are widely used for molecular recognition in biomarker assays. For optimal sensitivity and selectivity using gold platforms, a nearly atomically smooth (111) oriented Au surface is highly desirable and requires additional surface preparation by techniques such as template stripping or flame annealing. Thiolate SAMs are unstable in aqueous solutions, endure a very limited pH range and suffer from reductive desorption.[25] We use TiO_2 nanotube arrays without gold nanoparticles as assay platforms to perform the sensitive detection of troponin I by using bifunctional self-assembled monolayers of 16-phosphonohexadecanoic acid consisting of terminal -carboxylic acid and -phosphonic acid groups to immobilize biomolecules. Alkylphosphonic acid SAMs on TiO_2 are highly robust, durable and stable in aqueous solutions over a wide pH range from 2–10.[26] Similar to thiolate SAMs, long chain alkylphosphonic acids yield close-packed monolayers with a high grafting density of alkyl groups of 4.3–4.8 alkyl groups/nm^2 and a high degree of ordering of alkyl chains.[27] Carboxyalkyl phosphonic acid SAMs on TiO_2 have a more restricted chain mobility than related alkylphosphonic acid SAMs due to hydrogen bonding among the pendant –COOH groups.[28] Phosphonic acid ligands have a much higher affinity for TiO_2 surfaces than carboxylic groups[29] and selectively bind to TiO_2 surfaces. Due to strong interactions with the substrate, phosphonic acid SAMs are known to possess a higher hydrolytic stability than silane SAMs and require no surface conditioning to obtain high coverage. At room temperature, SAMs of octadecane phosphonic acid (ODPA) on TiO_2 showed only a 2–5% loss in grafting density after spending one week at pH 1–10.[26]

In this study we have developed a sensitive extended sandwich-type immunoassay consisting of three-dimensional nanotube arrays for the detection of human cardiac troponin (cTnI) since cTnI is considered the 'gold standard' in terms of diagnosing MI, owing to its presence only resulting from direct damage of myocardium.[30] Troponin I was captured on a self assembled monolayer of 16-phosphonohexadecanoic acid on TiO_2 surface using a polyclonal anti-goat troponin antibody. Antigen–primary antibody interaction was followed by conjugation with a secondary antibody (anti-mouse troponin). Subsequently, the secondary antibody was conjugated with a fluorophore labeled tertiary antibody, whose intensity of fluorescence was measured to determine the concentration of the cardiac troponin I. A detection limit of 0.1 pg ml^{-1} was achieved using the present immunoassay. In comparison, commercially available popular cTnI assays such as Abbott Labs' iStat and Beckman Coulter's Access assays for cTnI both have detection limits in approximately the 0.01 ng ml^{-1} range.[31] Roche Diagnostics' Elecsys assays human cardiac troponin T (cTnT) with a detection limit of ~0.01 ng ml^{-1}.[31]

2. Materials and methods

2.1 Anodic growth

Titanium dioxide (TiO_2) nanotube arrays were obtained by anodization of a 0.89 mm thick titanium foil (99.7%, Alfa Aesar) in a two-electrode anodization setup in which titanium foils were used as both the anode and cathode and only two-thirds of the length of titanium foil was immersed into the solution. The inter-electrode spacing was approximately 5 cm. Anodization was carried out at room temperature in an electrolyte consisting of a mixture of 3 wt% acetic acid (37% solution, Sigma Aldrich) and 0.25 wt % HF (48% solution, Sigma Aldrich), in deionized water under the applied voltage of 20V. The electrochemical cell had a closed lid to reduce variation in electrolyte concentration with time, and the anodization was performed inside a fume hood with the sash half-closed. After anodization, the titanium foils containing the nanotubes were rinsed with water, then isopropyl alcohol and dried in air. Further detailed procedures can be found elsewhere.[6] Longer nanotubes were obtained by anodizing Ti foils at room temperature in an electrolyte consisting of a mixture of ethylene glycol (Reagent plus 99%, Sigma Aldrich), NH_4F (98% A.C.S. reagent, Sigma Aldrich), and deionized water under the applied voltage of 40V. The electrolyte consisted of a solution of 0.5 wt% NH_4F and 2% (volume) deionized water in ethylene glycol. After anodization, the titanium foils containing the nanotubes were rinsed with water, then isopropyl alcohol and dried in air. The as-grown nanotubes had debris on the surface. They were cleaned by overnight immersion in 0.1M HCl followed by rinsing with water and subsequent sonication in water and isopropyl alcohol. Cleaner high surface area nanotubes were also grown by anodizing Ti foils at 7.5–60 V for 48 h in dimethyl sulfoxide (DMSO) electrolytes containing 2–3% water and 1–2% HF. These nanotubes were used as formed.

2.2 Characterization and detection

Imaging of the nanoscale morphology of the samples was performed using a JEOL 6301F cold cathode field emission scanning electron microscopy (FESEM) and a Zeiss Leo 1430 hot cathode SEM. The Fourier Transform Infrared (FTIR) spectra were

obtained using a Bruker Vertex 70 FTIR equipped with a liquid nitrogen cooled mercury cadmium telluride (MCT) detector and a Harrick AutoSeagull IRRAS attachment placed in the sample compartment. The samples were horizontally mounted in a nitrogen-purged sample chamber with the infrared beam impinging upon the sample surface at 85 degrees to the surface normal. All FTIR spectra were obtained with 500 scans in 800–4000cm^{-1} spectral region at 4 cm^{-1} resolution. Background spectra were obtained by using bare Ti foil in the same geometry. X-ray photoelectron spectroscopy (XPS) was performed using a Kratos XPS spectrometer with a Mono Al Kα X-ray source with Hv = 14 kV and Current = 15 mA. Survey sepectra were scanned with pass energy of 0.35 eV. High resolution spectra were scanned with pass energy of 0.1 eV. Fluorescence imaging was performed using a Li-Cor Odyssey Imaging System and a Zeiss LSM 710 laser scanning confocal fluorescence microscope.

2.3 Immunoassay protocols

2.3.1 Self-assembled monolayer of 16-phosphonohexadecanoic acid on TiO_2 nanotubes. SAMs of 16-PHA were prepared by incubating the TiO_2 nanotubes in 1 mM solution of 16-PHA in a mixture of ethanol and deionized water for 15 h at room temperature. With adsorbed phosphonic acid derivatives, it is known that control of the ratio of ethanol to water is key to obtaining a monolayer instead of an undesirable bilayer wherein the phosphonic group on the second layer is oriented toward the solution. In our case, we found a 1 : 4 mixture of water and ethanol to yield the best results. The TNA substrates were rinsed with 100% ethanol in order to remove any non-bonded chemicals. The process can be visualized in schematic of Fig. 1. The schematic is meant to be illustrative of the concept; in reality, the monolayer is coated on both the top surface as well as on the inner and outer walls of the nanotubes.

2.3.2 Activation of the monolayer. The monolayer was activated by using 1-ethyl-3-3-dimethylaminopropyl carbodiimide hydrochloride (EDC) and N-hydroxy-succiinimide (NHS) chemistry. EDC is a zero length cross-linker used to couple carboxyl groups to primary amines. The activation was done by adding 25mM EDC and 0.2mM of NHS in acetonitrile for 1 h followed by washing with ethanol.

2.3.3 Verification of protein immobilization on 16-PHA functionalized TiO_2 nanotube arrays. After activating TiO_2 nanotube arrays with 16 PHA, they were treated with EDC and NHS to activate the amine group. This was followed by IgG testing of the nanotube arrays. This test consisted of TiO_2 nanotube array samples, blocking agent (BSA), and anti-mouse fluorescence. The control samples consisted of TiO_2 nanotube array samples blocked by BSA immediately following the activation step, which was then followed by immersion in a solution of the fluorescent dye-tagged anti-mouse IgG. The verification samples consisted of activated nanotubes on which anti-mouse fluorescence was directly immobilized.

2.3.4 Primary antibody immobilization. A solution of 20μg ml^{-1} anti-goat troponin in phosphate buffer solution (PBS) was applied to activate TiO_2 nanotubes by using a micropipette for 1 h. After that, the sample was rinsed with PBS three times to remove any unbound antibodies on the surfaces.

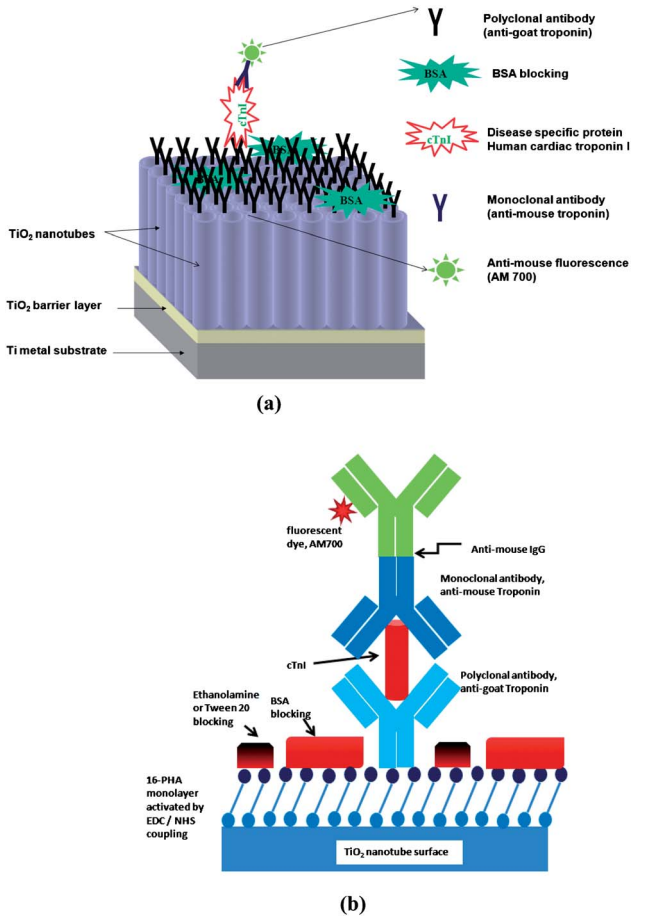

Fig. 1 (a) Schematic diagram of assays based on TiO_2 nanotubes. In brief, antibodies which recognize the specific protein (Troponin I) binds to monoclonal antibody specific to the troponin protein and then detection is achieved by secondary antibody which is anti-mouse fluorescence. (b) Magnified schematic of the binding processes close to the nanotube surface.

2.3.5 Troponin immobilization. After blocking, different concentrations (0.1 pg ml^{-1}-100 ng ml^{-1}) of human cardiac troponin I were prepared and immobilized on the antibody immobilized TiO_2 nanotube surfaces. 100 μL of analyte containing troponin was applied on the TNAs using a micropipette for an incubation period of 2 h followed by rinsing with PBS and drying in air.

2.3.6 Bovine serum albumin (BSA) blocking. This step was performed in order to prevent any non-specific binding to the amine-terminated SAM in sample areas, if any, where primary antibodies were not present. A solution of 1% BSA was applied to the Troponin bound TiO_2 nanotubes samples for 30 min followed by rinsing with PBS. To detect lower troponin concentrations (<0.1 ng mL^{-1}), a two-step blocking process was employed. The two step blocking process was achieved by using two different procedures. In one procedure, 1M ethanolamine at

pH 9 was applied, and in the other, 0.5 vol. % Tween 20 in PBS at pH 7.4 was applied, for 1 h followed by application of 1% BSA for 1 h. Ethanolamine (or Tween 20) being the primary blocker to passivate unreacted carboxyl groups and 1% BSA for one hour was used as the secondary blocker to block non-specific binding sites.

2.3.7 Secondary antibody immobilization. In this step different anti-mouse antibody was functionalized on the troponin attached to the TiO_2 nanotubes *via* the linkage to the immobilized primary antibody. A solution of 20 μg ml^{-1} anti-mouse was applied to the above sample by a micropipette for 30 min followed by rinsing with PBS and drying in air.

2.3.8 Binding of fluorescence tagged tertiary antibody. In this final step the anti-mouse fluorescence (AM700) was added for 30 min followed by rinsing with PBS to rinse out any unbound AM700. In the control experiment, all steps were identical except that the troponin step and secondary antibody immobilization were omitted, and PBS was added instead. This step was to confirm the binding of antibody on the activated TiO_2 monolayer.

3. Results and discussions

3.1 Morphology of TiO_2 nanotubes

Fig. 2a shows the field emission scanning electron microscopy (FESEM) image of as grown TiO_2 nanotubes arrays at anodization voltage of 20V for 45 min. Fig. 2a shows that the nanotubes are aligned and close-packed. The average diameter of these nanotubes is 76 nm and a length of ~400nm was observed. Nanotubes can be grown very quickly (30–45 min) using unbuffered HF-based recipes in aqueous electrolytes. A detection limit of 0.1 ng ml^{-1} was achieved using these nanotubes, with higher sensitivities limited by the relatively low aspect ratio (~4) and correspondingly low surface area (~25 times a flat planar surface). To extend the sensitivity of our assay beyond 0.1 ng ml^{-1}, we used longer nanotubes (shown in Fig. 2b) grown in ethylene glycol (EG)-based electrolytes and dimethyl sulfoxide (DMSO)-based electrolytes as platforms for molecular recognition to enable a larger effective surface area for protein immobilization. However, nanotubes longer than 5 μm grown in EG-based electrolytes suffer from anodization debris covering the surface and clogging the pores. Such debris can be removed by extended ultrasonication of the nanotube samples. However the ultrasonic cleaning process also results in breakage of nanotubes, due to which the average nanotube lengths change significantly and identical samples become difficult to reproduce. On the other hand, nanotubes grown in HF-containing (DMSO) electrolytes are characterized by slow growth rates but a very clean morphology requiring little additional cleaning. DMSO-grown nanotubes, which are shown in Fig. 3 are also reproducible in quality.

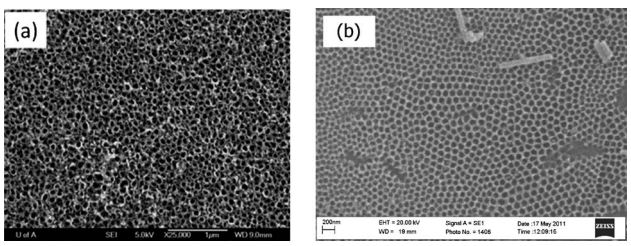

Fig. 2 SEM images of the top-view of (a) TiO_2 nanotubes formed by anodization at 20 V in aqueous electrolyte and (b) TiO_2 nanotubes formed by anodization at 40 V in EG-based electrolyte.

3.2 Monolayer characterization

Characterization of the monolayer was done using XPS and FTIR at each step. Fig. 4 (a) and (b) show the FTIR data after SAM formation and after monolayer activation respectively. In each case, the two features around 2850 and 2940 cm^{-1} are assigned to the CH_2 symmetric and CH_2 asymmetric modes from the carbon backbone respectively. In the case of FTIR data after EDC/NHS activation, the three characteristic bands at ~1815, 1790 and 1750 cm^{-1} correspond to the carbonyl stretch modes in the COO-NHS ester moiety.[14,18]

The monolayer in our case is a bifunctional molecule, namely 16-phosphonohexadecanoic acid which is terminated with a carboxylic group at one end and a phosphonic group at the other. In Fig. 4(a), peak at 1694 cm^{-1} indicates the carboxylic group present at the monolayer. Spectral interference due to the broad peak at ~1000 cm^{-1} obscures phosphonic group identification in this region. In Fig. 4(b) the appearance of the carbonyl peak at 1698cm^{-1} is indicative of the presence of amide I carbonyl stretching mode resulting from 1,2-diamineoethane attachment. Peaks at 1280 cm^{-1} and 1242 cm^{-1} correspond to C–OH stretch mode and C–N–C succycle anti-symmetric CNC stretching mode. The peak at 1560 cm^{-1} belongs to peptide N–H bending of amide II.[19,20]

XPS spectra acquired for monolayer coated on TiO_2 surface is shown in Fig. 5. Fig. 5(a) shows the survey spectrum for monolayer coated TiO_2 nanotube surface. This clearly shows the P2s peak at 191eV and P 2p peak at 134 eV core lines which are consistent with PO_3 compounds[21] in addition to C 1s at 285eV

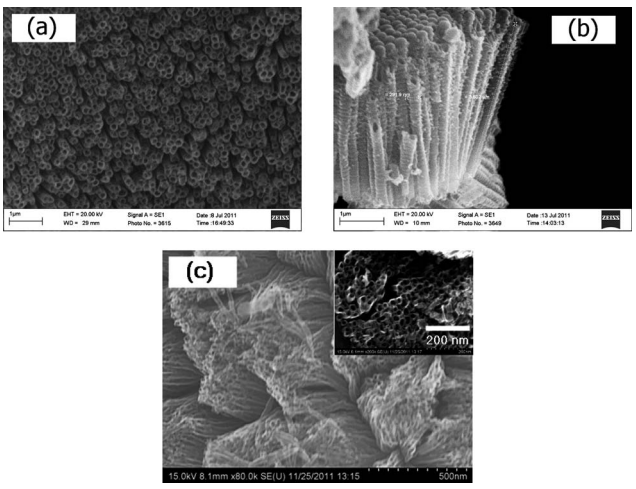

Fig. 3 SEM images of (a) top-view (b) cross-section of TiO_2 nanotubes formed by anodization at 60 V in DMSO-based electrolyte and (c) top-view (b) top-view of TiO_2 nanotubes formed by anodization at 7.5 V in DMSO-based electrolyte.

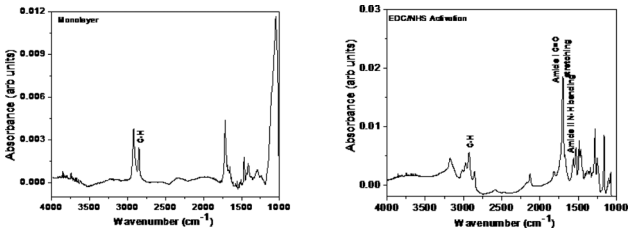

Fig. 4 FTIR spectra of TiO_2 nanotubes (a) after monolayer formation and (b) after EDC/NHS activation.

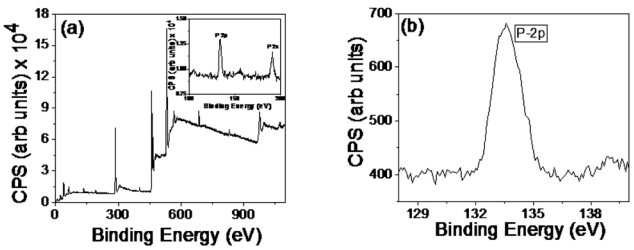

Fig. 5 XPS scans of monolayer (16-phosphonohexadecanoic acid) on TiO_2 nanotubes surface (a) survey scans and inset shows P 2s and P 2p and (b) high resolution scan of P 2p region.

and several other peaks. Both P 2s and P 2p peaks are observed in the survey scan and a clear peak is found in the high resolution scan of P 2p region for monolayer coated TiO_2 nanotubes surface (Fig. 5b). These results positively demonstrate the presence of phosphonic acid head group on top surface of TiO_2 nanotubes.

3.3 Fluorescence detection

Every single sample that was assayed was associated with a corresponding control sample prepared in the same run under identical conditions. As mentioned previously, we performed two-step IgG testing to verify protein immobilization. For extended sandwich-type troponin assays, solutions containing various concentrations of human cardiac troponin I (from 100 ng ml^{-1} to 0.01 pg ml^{-1}) were used. We used fluorescence scanning microscopy to check the intensity of fluorescence from the functionalized nanotube array samples at different concentrations of troponin. A ratio of at least 4 of the fluorescence intensity of the assayed sample to that of the control samples (S/N threshold = 4) was used to detect cTnI. The use of polyclonal antibodies (see Fig. 1) as probes to capture troponin results in high sensitivity due to binding to multiple epitopes.

Using short nanotubes grown in aqueous electrolytes with pore-sizes of ~76 nm and lengths of 400 nm, 0.1 ng ml^{-1} was the lowest concentration which could be detected using our S/N threshold of 4. The intensity value-labeled fluorescent images for 100 ng ml^{-1}, 10 ng ml^{-1} and 1 ng ml^{-1} are shown in Fig. S1 in Supporting Information. The fluorescence intensities obtained for different troponin concentrations in the range of 0.1–100 ng ml^{-1} using identical scan settings were normalized to the same sample area and are presented in tabular format in Table S2 in Supporting information. Nanotubes grown in EG-based electrolyte had a pore size of ~70 nm and a tube-length of 10 μm. As mentioned previously, the sensitivity of EG-grown nanotubes was limited by the pore-clogging debris on the surface and such samples were therefore useful for sensing cTnI concentrations only up to 0.05 ng ml^{-1}. Fig. S3 shows that the S/N ratio obtained with EG-grown nanotubes is higher than the detection threshold for 0.05 ng ml^{-1} but lower than 4 for a troponin concentration of 0.01 ng ml^{-1}. On the other hand DMSO-grown nanotubes of length ~4 μm were relatively clean and their diameter was tuned by adjusting the anodization voltage over the range 7.5 V–60 V. An anodization voltage of 60 V resulted in a diameter of 270 nm while a voltage of 7.5 V resulted in a diameter of 30 nm. Fig. 6 shows the lowest concentrations of troponin detected by our TiO_2 nanotube array fluorescent immunoassay.

In making these measurements, we also tested our samples for troponin zero in each case. For troponin zero, we used phosphate buffer solution containing no troponin. For troponin zero, there was a very low signal observed as compared to different concentrations of troponin. Most other fluorimetric assays have high noise due to significant background fluorescence. The low background fluorescence in our nanotube array platform is one of the factors contributing to the achievement of high sensitivities. Non-specific binding due to biofouling is a major obstacle limiting sensitivities in assays based on planar gold platforms, in reaction to which mixed monolayers of polyethylene glycol (PEG)-terminated and carboxylic acid-terminated self-assembled monolayers are often used.[32] We were able to obtain high sensitivities without enzymatic amplification using a single component fully hydrophilic long-chain carboxylic acid-terminated monolayer. In order to detect troponin concentrations lower than 0.1 ng ml^{-1}, a single step blocking process using bovine serum albumin was found to be insufficient. We developed a highly effective two-step blocking process using ethanolamine or Tween 20 surfactant as the primary blocker and 1% BSA as the secondary blocker. At 0.5 pg ml^{-1}, blocking with Tween 20 enabled higher S/N ratios than with ethanolamine as shown in Fig. 6 (a). Additional fluorescence images examining the efficacy of the blocking process are shown in Figs. S4–S6. The trend observed was that a two-step process consisting of blocking by Tween 20 and subsequently by BSA, provided the best S/N ratio. Also, the two-step process consisting of blocking by ethanolamine and subsequently by BSA outperformed the single step BSA blocking process. Our results indicate that the best

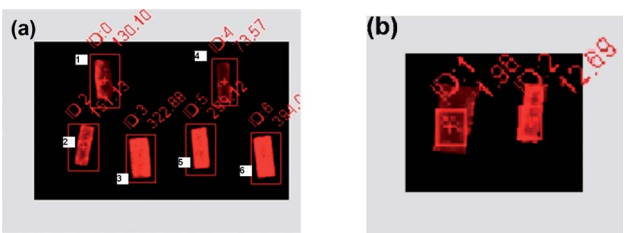

Fig. 6 (a) and (b) Fluorescence images of a troponin immunoassay using TiO_2 NT array samples grown in DMSO electrolyte by anodization at 7.5 V. (a) shows Troponin concentrations of (1) 0 pg ml^{-1}, (2) 0.5 pg ml^{-1} (3) 1 pg ml^{-1} (4) 0 pg ml^{-1} (5) 0.5 pg ml^{-1} and (6) 1 pg ml^{-1}. In each case, a two-step blocking process was used with 1% BSA as the secondary block. For the primary block, ethanolamine was used for samples (1), (2) and (3) while Tween 20 was used for samples (4), (5) and (6). (b) shows Troponin concentration of 0 pg ml^{-1} (left) and 0.1 pg ml^{-1} (right), where blocking process was implemented using Tween 20 followed by 1% BSA.

blocking process not only minimizes non-specific binding but also causes the least disruption to the binding of antigen to the immobilized antibody. Furthermore, as can be observed from Fig. 6 (b), a detection limit of 0.1 pg ml^{-1} of Troponin is achievable by using the two-step blocking process and TiO_2 nanotubes anodized in DMSO electrolyte at 7.5 V. Since a lower anodization voltage results in a smaller pore diameter, 7.5 V-anodized nanotubes have the smallest inner diameters of all the nanotubes used in this study. This suggests that the ability of the unique topography of nanotube and nanowire arrays to resist biofouling[33,34] may explain the reduced propensity for non-specific binding on nanotube array platforms in the results obtained by us and by Song *et al.*[9] Another factor is the use of polyclonal primary antibodies to capture troponin molecules in solution. At very low troponin concentrations, any one of several epitopes on cTnI may be recognized by the polyclonal antibodies for binding to occur, thus increasing the chances of capture of the few cTnI molecules in solution. A third factor is the high surface area of the nanotube array platform. The sensitivity of the assay is primarily a function of the total number of active sites available to capture troponin molecules in solution, and is consequently directly related to the surface area of the nanotubes. The low limit of detection of the assay can be improved by increasing the surface-to-volume ratio of the platform. Thus, high aspect ratio nanotube arrays grown in DMSO electrolytes over longer anodization durations significantly outperform shorter NT arrays formed in aqueous electrolytes.

Using the average dimensions of DMSO-grown nanotubes obtained by FESEM images, we infer a nanotube density of $\sim 2 \times 10^9$ cm^{-2}. Since each nanotube has a geometric surface area of $\sim 10^7$ nm^2, and since the approximate size of the troponin and anti-troponin molecules are 200 nm^2, the maximum possible coverage of proteins on the surface assuming close-packing is calculated to be 10^{14} molecules and the number of activated carboxyl group binding sites is at least two-three orders higher. It is this high surface area which enables the exquisite sensitivity of the nanotube array platform, provided non-specific binding is minimized. Our calculations indicate that for troponin concentrations at the detection limit of our study, there are $\sim 10^5$ troponin molecules present in the solution exposed to the nanotubes, which are subsequently bound and detected. Since Fig. 6 (b) show a significant S/N ratio >4 at this concentration, our results point to the possibility of further optimizing TNAs. The final objective would be the achievement of single molecule sensitivity.[35–40]

The average normalized fluorescence intensity for assays using short NTs formed in aqueous electrolytes increased roughly linearly with concentration in the 0.1 ng ml^{-1}–1 ng ml^{-1} range from 3.87 to 26.89 in increments of approximately 2.5 counts for every 0.1 ng ml^{-1} increase in concentration as shown in Table S3. However, the standard deviations of the intensities significantly exceeded the average concentration due to which close-lying concentrations of troponin were difficult to resolve. For concentrations higher than 1 ng ml^{-1}, the intensity increases more slowly in a non-linear fashion. Since the fluorescence imaging system provides the integrated fluorescence intensity at each pixel on the surface, the contribution of the troponin molecules closest to the surface is weighted most strongly and inner filter effects also result in a non-linear response such as obtained by us. Binding sites at, or close to the top surface of the nanotubes are most easily accessible to the troponin molecules in solution and are therefore saturated at relatively low troponin concentrations. Because of the ability of confocal microscopy to eliminate light from the plane other than the focal plane, it provides us a better indication of the density and distribution of fluorophores in the sample for different analyte concentrations. We used laser scanning confocal microscopy to more clearly amplify the differences between different concentration ranges. Fig. 7 shows the confocal images for three different aqueous nanotube array samples exposed to 100 ng ml^{-1}, 1 ng ml^{-1} and 0.1 ng ml^{-1} of troponin respectively. These images were taken while keeping all microscope settings and imaging parameters identical. It can be clearly seen that a very large percentage of the active binding sites are occupied by fluorophores in the 100 ng ml^{-1} sample whereas with 10 ng ml^{-1}, a much smaller percentage of binding sites are occupied. Fig. 8 shows the confocal images for DMSO-grown nanotube array samples exposed to 10 pg ml^{-1}, 1 pg ml^{-1} and 10 ng ml^{-1} of troponin in comparison with a control sample.

Our results provide important insights on controlling the sensitivity and responsivity of TiO_2 nanotubes. Higher surface areas and concomitantly higher sensitivities may be obtained by making the nanotube diameters smaller and by increasing the nanotube length. Furthermore, a nanotube architecture of a given surface area has a characteristic range of detection where the intensity response is a linear function of concentration. This suggests that choosing a set of distinct tailored nanotube array architectures, a linear range of detection appropriate to the specific application may be obtained. The large % standard deviation in the fluorescence intensity counts may be reduced by improving the quality and pattern order of the nanotube arrays and also by ensuring more uniform mass transport of the troponin molecules in the nanochannels. The dynamic range of

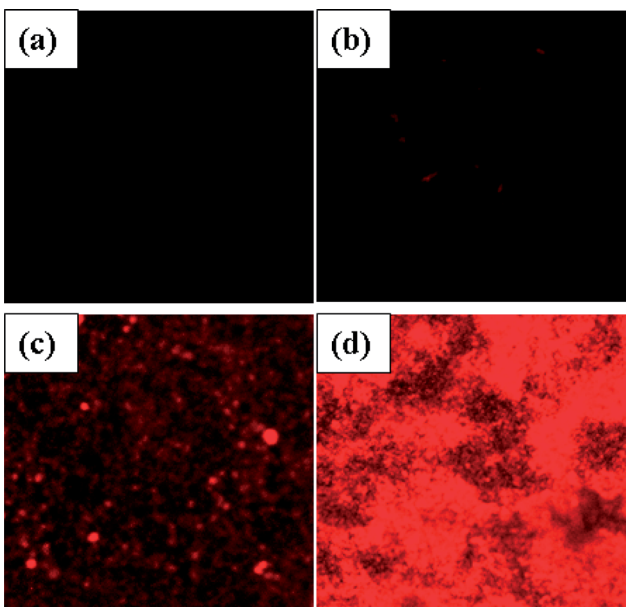

Fig. 7 Confocal fluorescence microscope images of aqueous nanotubes stained with AM700 of (a) bare TiO_2 nanotubes, and troponin concentrations of (b) 0 ng ml^{-1}, (c) 10 ng ml^{-1} and (d) 100 ng ml^{-1}.

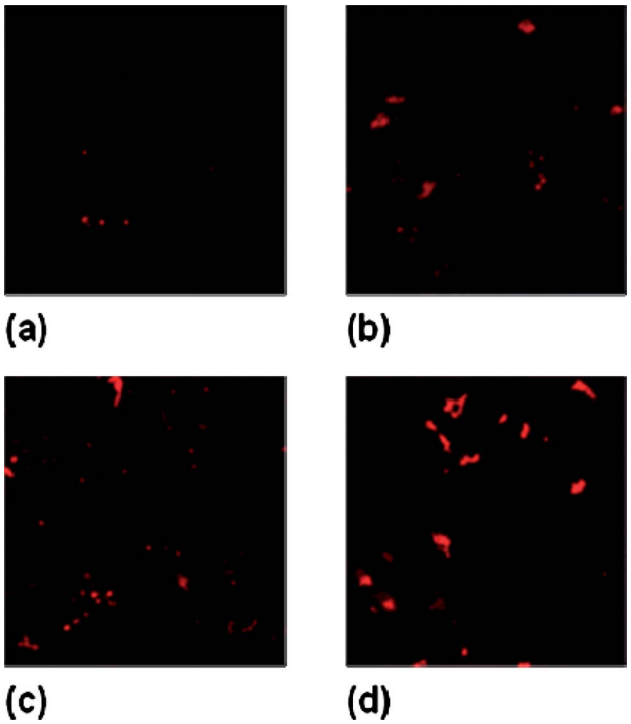

Fig. 8 Confocal fluorescence microscope images of nanotubes formed by anodization in the DMSO electrolyte at 15 V for troponin concentrations of (a) 0 pg ml^{-1}, (b) 1 pg ml^{-1}, (c) 10 pg ml^{-1} and (d) 10 ng ml^{-1}. In each case, two-step blocking using 1M ethanolamine followed by 1% BSA was used.

the assay is limited by saturation of the intensities, which can be reduced by decreasing the sample volume used, by using monoclonal capture antibodies and by reducing the amount of time nanotubes are exposed to troponin solutions.

Conclusion

In summary, we have demonstrated an ultrasensitive immunoassay capable of detecting troponin concentrations as low as 0.1 pg ml^{-1} using a TiO_2 nanotube array platform without the use of enzymatic amplification. A carboxyalkylphosphonic acid monolayer on the TiO_2 surface coupled with a two-step blocking sequence to minimize non-specific binding were found to be critical for achieving high sensitivities. The highest S/N ratio was obtained for a two-step blocking process consisting of Tween 20 and BSA. The very low detection limit is promising for the achievement of high resolution measurements in the physiologically important concentration range of 0.01 ng ml^{-1} to 10 ng ml^{-1}. The use of tailored and optimized TiO_2 nanotubes in microwells could extend the detection range of commercially available point of care troponin assays, most of which use ELISA-based principles and/or luminescence detection.[30,41,42]

Acknowledgements

We thank NSERC and CIHR for funding support. Our sincere thanks to Wayne Moffat and Craig Turk at the Analytical and Instrumentation Laboratory for assistance with FTIR data collection and analysis, and to Jun Ren and Xiuqing Ding for assistance with assay design. We would like to acknowledge the assistance provided by Dimitre Karpuzov at the Alberta Centre for Surface Engineering and Science (ACSES) in the collection of XPS data. We thank Scott at the Alberta Nanofab and De-Ann Rollings in the Department of Earth and Atmospheric Sciences for help with SEM. We also thank Dr Xuejun Sun at the Cross Cancer Institute for helpful discussions with regard to optical imaging.

References

1 R. Twerenbold, T. Reichlina, M. Reiter and C. Mueller, *Swiss Med. Wkly.*, 2011, **141**.
2 M. Gustapane, G. Biasillo, R. Della Bona and L. M. Biasucci, *Minerva Med.*, 2011, **102**, 161–168.
3 L. Aihua, *Biosens. Bioelectron.*, 2008, **24**, 167–177.
4 J. Wang, *ChemPhysChem*, 2009, **10**, 1748–1755.
5 A. Star, E. Tu, J. Niemann, J. C. P. Gabriel, C. S. Joiner and C. Valcke, *Proc. Natl. Acad. Sci. U. S. A.*, 2006, **103**, 921–926.
6 G. F. Zheng, F. Patolsky, Y. Cui, W. U. Wang and C. M. Lieber, *Nat. Biotechnol.*, 2005, **23**, 1294–1301.
7 K. S. Mun, S. D. Alvarez, W. Y. Choi and M. J. Sailor, *ACS Nano*, 2010, **4**, 2070–2076.
8 A. Mohammadpour and K. Shankar, *J. Mater. Chem.*, **20**, pp. 8474–8477.
9 Y. Y. Song, F. Schmidt-Stein, S. Berger and P. Schmuki, *Small*, 2010, **6**, 1180–1184.
10 Y. R. An, L. L. Tang, X. L. Jiang, H. Chen, M. C. Yang, L. T. Jin, S. P. Zhang, C. G. Wang and W. Zhang, *Chem.–Eur. J.*, 2010, **16**, 14439–14446.
11 K. C. Popat, M. Eltgroth, T. J. LaTempa, C. A. Grimes and T. A. Desai, *Biomaterials*, 2007, **28**, 4880–4888.
12 K. C. Popat, L. Leoni, C. A. Grimes and T. A. Desai, *Biomaterials*, 2007, **28**, 3188–3197.
13 K. C. Popat, M. Eltgroth, T. J. La Tempa, C. A. Grimes and T. A. Desai, *Small*, 2007, **3**, 1878–1881.
14 S. Oh, K. S. Brammer, Y. S. J. Li, D. Teng, A. J. Engler, S. Chien and S. Jin, *Proc. Natl. Acad. Sci. U. S. A.*, 2009, **106**, 2130–2135.
15 J. Park, S. Bauer, K. von der Mark and P. Schmuki, *Nano Lett.*, 2007, **7**, 1686–1691.
16 M. Paulose, L. Peng, K. C. Popat, O. K. Varghese, T. J. LaTempa, N. Z. Bao, T. A. Desai and C. A. Grimes, *J. Membr. Sci.*, 2008, **319**, 199–205.
17 S. C. Roy, M. Paulose and C. A. Grimes, *Biomaterials*, 2007, **28**, 4667–4672.
18 in *ScienceDaily*, 2011.
19 T. A. Leski, A. P. Malanoski, D. A. Stenger and B. C. Lin, *Future Microbiol.*, 2006, **5**, 191–203.
20 S. Dhawan, *Expert Rev. Mol. Diagn.*, 2006, **6**, 749–760.
21 P. Scrimin and L. J. Prins, *Chemical Society Reviews*.
22 Z. J. Zhang, Y. B. Xie, Z. Liu, F. Rong, Y. Wang and D. G. Fu, *J. Electroanal. Chem.*, 2011, **650**, 241–247.
23 A. W. Zhu, Y. P. Luo and Y. Tian, *Anal. Chem.*, 2009, **81**, 7243–7247.
24 P. L. Truong, C. Cao, S. Park, M. Kim and S. J. Sim, *Lab Chip*, 2011, **11**, 2591–2597.
25 N. T. Flynn, T. N. T. Tran, M. J. Cima and R. Langer, *Langmuir*, 2003, **19**, 10909–10915.
26 S. Marcinko and A. Y. Fadeev, *Langmuir*, 2004, **20**, 2270–2273.
27 R. Helmy and A. Y. Fadeev, *Langmuir*, 2002, **18**, 8924–8928.
28 S. Pawsey, K. Yach and L. Reven, *Langmuir*, 2002, **18**, 5205–5212.
29 J. P. Folkers, C. B. Gorman, P. E. Laibinis, S. Buchholz, G. M. Whitesides and R. G. Nuzzo, *Langmuir*, 1995, **11**, 813–824.
30 M. I. Mohammed and M. P. Y. Desmulliez, *Lab Chip*, 2011, **11**, 569–595.
31 J. R. Tate and M. Panteghini, *Biochimica Clinica*, 2008, **32**, 535–546.
32 M. J. Shuster, A. Vaish, M. E. Szapacs, M. E. Anderson, P. S. Weiss and A. M. Andrews, *Adv. Mater.*, 2008, **20**, 164.
33 K. M. Ainslie, G. Sharma, M. A. Dyer, C. A. Grimes and M. V. Pishko, *Nano Lett.*, 2005, **5**, 1852–1856.
34 J. Genzer and K. Efimenko, *Biofouling*, 2006, **22**, 339–360.

35 H. Harma, T. Soukka, S. Lonnberg, J. Paukkunen, P. Tarkkinen and T. Lovgren, *Luminescence*, 2000, **15**, 351–355.
36 J. W. Li, W. J. Xie, N. Fang and E. S. Yeung, *Anal. Bioanal. Chem.*, 2009, **394**, 489–497.
37 D. M. Rissin, D. R. Fournier, T. Piech, C. W. Kan, T. G. Campbell, L. A. Song, L. Chang, A. J. Rivnak, P. P. Patel, G. K. Provuncher, E. P. Ferrell, S. C. Howes, B. A. Pink, K. A. Minnehan, D. H. Wilson and D. C. Duffy, *Anal. Chem.*, 2011, **83**, 2279–2285.
38 R. Schmidt, J. Jacak, C. Schirwitz, V. Stadler, G. Michel, N. Marme, G. J. Schutz, J. D. Hoheisel and J. P. Knemeyert, *J. Proteome Res.*, 2011, **10**, 1316–1322.
39 L. A. Tessler, C. D. Donahoe, D. J. Garcia, Y. S. Jun, D. L. Elbert and R. D. Mitra, *J. R. Soc. Interface*, 2011, **8**, 1400–1408.
40 S. Y. Tetin, K. M. Swift and E. D. Matayoshi, *Anal. Biochem.*, 2002, **307**, 84–91.
41 D. Bottenus, T. Z. Jubery, Y. X. Ouyang, W. J. Dong, P. Dutta and C. F. Ivory, *Lab Chip*, 2011, **11**, 890–898.
42 D. M. Bruls, T. H. Evers, J. A. H. Kahlman, P. J. W. van Lankvelt, M. Ovsyanko, E. G. M. Pelssers, J. Schleipen, F. K. de Theije, C. A. Verschuren, T. van der Wijk, J. B. A. van Zon, W. U. Dittmer, A. H. J. Immink, J. H. Nieuwenhuis and M. W. J. Prins, *Lab Chip*, 2009, **9**, 3504–3510.

